

Klein paradox and resonant tunneling in a graphene superlattice

Chunxu Bai and Xiangdong Zhang*

Department of Physics, Beijing Normal University, Beijing 100875, China

(Received 2 March 2007; revised manuscript received 2 June 2007; published 28 August 2007)

This paper studies the transport properties of charge carriers through graphene superlattices consisting of monolayer or bilayer graphene on the basis of the transfer-matrix method. Emphasis is placed on the relationship between the Klein paradox and resonant tunneling in double-barrier junctions. It is shown that normal incidence transmission probabilities for two kinds of graphene structure exhibit different features. Independent of structure parameters, they are always perfectly transmitted in a monolayer graphene structure. In contrast, the transmission resonances occur in a bilayer graphene structure. However, the angularly averaged conductivities for both depend on the thickness and height of the barriers as well as the width and number of the well. That is to say, the angularly averaged conductivities in monolayer and bilayer graphene superlattices can be controlled by changing the structure parameters even if Klein tunneling exists.

DOI: [10.1103/PhysRevB.76.075430](https://doi.org/10.1103/PhysRevB.76.075430)

PACS number(s): 73.43.Cd, 81.05.Uw, 73.63.Bd

I. INTRODUCTION

Recently, great interest has been aroused in research on the physical properties of graphene due to the successful fabrication experiment by Novoselov *et al.*¹ Graphene is a monolayer of carbon atoms densely packed in a honeycomb lattice, which can be viewed as either an individual atomic plane pulled out of bulk graphite or unrolled single-wall carbon nanotubes. In graphene, the energy bands can be described at low energy by a two-dimensional Dirac equation centered on hexagonal corners (Dirac points) of the honeycomb lattice Brillouin zone.^{2,3} The quasiparticle excitations around the Dirac point obey linear Dirac-like energy dispersion. The presence of such Dirac-like quasiparticles is expected to lead to a number of unusual electronic properties in graphene such as unconventional quantum Hall effect,^{4–8} strong electric-field effect,⁹ finite minimal conductivity,^{4,10} special Andreev reflection,^{11,12} and so on. It is also interesting that the presence of such quasiparticles in graphene can provide us with an experimental test for the Klein paradox.^{13,14}

The Klein paradox describes a tunneling phenomenon of a relativistic electron through a high potential barrier.^{13–18} It predicts that the electron can pass through the high potential barrier to approach the perfect transmission in contrast to the conventional nonrelativistic tunneling where the transmission probability exponentially decays with the increasing of the barrier height.^{15–18} This relativistic effect can be interpreted in the framework of Dirac's hole theory as a manifestation of the generation of positron-electron pairs.^{15–18} Although the Klein paradox was understood several decades ago, it has never been observed experimentally. Indeed, to observe it requires a very high potential drop and it becomes almost impossible to realize in general solid-state systems. It is only expected to occur in the high energy systems. Very recently, however, Katsnelson *et al.*¹³ proposed an experimental realization of the prediction of the Klein paradox by using electrostatic barriers in a two-dimensional monolayer or bilayer graphene. They have designed an experimental setup and demonstrated theoretically that the effect can be tested in the graphene systems.

However, their research on the Klein paradox in the graphene systems is only applicable to the single-barrier junction. It is well-known that transport of an electron described by the Schrödinger equation in the semiconductor superlattice (Kronig-Penney-like model) can exhibit different features as compared with those in a single-barrier junction. Now, transport of an electron in monolayer graphene needs to be described by the Dirac-like equation. Then comes a problem: can any new features exhibit when Dirac fermions or bilayer graphene fermions are transmitted through graphene superlattices in contrast to single-barrier junction? In view of this problem, we extend in this paper the studies on a single-barrier junction¹³ into graphene superlattices consisting of monolayer or bilayer graphene by using the transfer-matrix method. The transmission probability and conductivity for these systems will be calculated, and the relationship between the Klein paradox and transport properties of charge carriers through two kinds of superlattices will be discussed. The rest of the paper is organized as follows: we will describe the theory and method in Sec. II, present the results and discussion in Sec. III, and give a summary in Sec. IV.

II. THEORY AND MODEL

We consider two kinds of superlattice, each consisting respectively of monolayer graphene or bilayer graphene. The schematic potential of electron and hole for the monolayer graphene superlattice is shown in Fig. 1. The system consists of two kinds of monolayer graphene strip alternately. The coordinate of the i th interface is marked by $l_{(i)}$. The growth direction is taken as the x axis, which is termed as the superlattice axis. We focus here on the case where the width (along the y direction) of the graphene strip, w , is much larger than $(l_{(i+1)} - l_{(i)})$ [$(l_{(i+1)} - l_{(i)}) \ll w$]. In this case, details of the microscopic description of the strip edges become irrelevant.

The top subgraph in Fig. 1 shows schematic diagrams of the spectrum of quasiparticles in a monolayer graphene structure. Due to the difference of Fermi energy and band structure between two monolayer graphene strips, the poten-

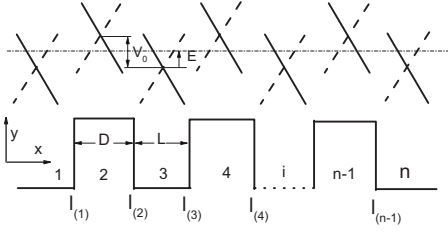


FIG. 1. Potential profile of quasiparticle transport in the monolayer graphene superlattice. The top picture corresponds to the schematic diagrams of the spectrum of the quasiparticles in different monolayers. The spectrums of electron and hole are linear. The solid and dashed lines emphasize the origin of the linear spectrum, which is the crossing between the energy bands associated with crystal sublattices. The cross points represent the Dirac points.

tial profile of the system is the multiple quantum well structure which is given by

$$V(x) = \begin{cases} V_0, & l_{(2i-1)} < |x| < l_{(2i)}, \quad i = 1, 2, \dots \\ 0, & \text{otherwise.} \end{cases} \quad (1)$$

This is similar to the potential profile of the semiconductor superlattice. The difference between them is that the charge carriers in the present system are described by the following Dirac-like equation rather than the usual Schrödinger equation.

$$\hat{H} = -i\hbar v_F \sigma \nabla + V(x), \quad (2)$$

where $v_F \approx 10^6 \text{ ms}^{-1}$ is the Fermi velocity, and $\sigma = (\sigma_x, \sigma_y)$ are the Pauli matrices. The electrons and holes in the semiconductor superlattice are normally described by separate Schrödinger equations, which are not in any way connected. In contrast, electron and hole states in the graphene superlattice are interconnected, exhibiting chiral properties. They are described by two-component wave functions (spinor wave functions).

If the monolayer graphene is replaced by the bilayer graphene in the above system, it becomes the bilayer graphene superlattice. There are some basic differences and similarities between them. The charge carriers in the bilayer graphene have a parabolic energy spectrum, which means they are massive quasiparticles with a finite density of states at zero energy, similar to conventional nonrelativistic electrons. They are described by the following off-diagonal Hamiltonian:¹³

$$\hat{H} = -\frac{\hbar^2}{2m} \begin{pmatrix} 0 & (k_x - ik_y)^2 \\ (k_x + ik_y)^2 & 0 \end{pmatrix} + V(x), \quad (3)$$

where k_x and k_y are the wave vectors along the x and y directions, respectively. On the other hand, these quasiparticles are also chiral and described by spinor wave functions, similar to relativistic particles or quasiparticles in the monolayer graphene.

A. Tunneling in monolayer graphene superlattice

In order to solve the transport problem in a monolayer graphene superlattice (sketched in Fig. 1), we assume that the incident electron wave propagates at an angle ϕ along the x axis. The general solution to Eq. (2) can be expressed as

$$\varphi_1(x, y) = (a_i e^{ik_{ix}x} + b_i e^{-ik_{ix}x}) e^{ik_y y},$$

$$\varphi_2(x, y) = s_i (a_i e^{ik_{ix}x + i\phi_i} - b_i e^{-ik_{ix}x - i\phi_i}) e^{ik_y y}. \quad (4)$$

Here $\varphi_1(x, y)$ and $\varphi_2(x, y)$ represent the components of the Dirac spinor in the i th monolayer graphene strip, where a_i and b_i are the transmission amplitudes, and

$$s_i = \text{sgn}(E - V_i), \quad k_{ix} = \frac{|E - V_i|}{\hbar v_F} \cos(\phi_i),$$

$$k_{iy} = \frac{|E - V_i|}{\hbar v_F} \sin(\phi_i).$$

Upon applying the continuity of the wave function at the boundaries, the following transfer matrix is obtained:

$$\begin{pmatrix} 1 \\ b_1 \end{pmatrix} = \frac{1}{1 + e^{2i\phi}} \begin{pmatrix} 1 - e^{i(\phi+\theta)} & 1 + e^{-i(\theta-\phi)} \\ e^{2i\phi} + e^{i(\theta+\phi)} & e^{-i(\theta-\phi)}(-1 + e^{i(\theta+\phi)}) \end{pmatrix} S(z) \\ \times \begin{pmatrix} e^{ik_x l(n)}(e^{-i\theta} - e^{i\phi})/[2e^{iq_x l(n)} \cos(\theta)] \\ e^{ik_x l(n)}(e^{i\theta} + e^{i\phi})/[2e^{-iq_x l(n)} \cos(\theta)] \end{pmatrix} a_{(n)}, \quad (5)$$

with $S(z) = S(z=l_{(2)})S(z=l_{(3)}) \cdots S(z=l_{(i)}) \cdots S(z=l_{(n-1)})$,

$$S(z=l_{(i)}) = \begin{pmatrix} t_{11} & t_{12} \\ t_{21} & t_{22} \end{pmatrix}, \quad (6)$$

$$t_{11} = e^{ik(i-1)l_{(i)}}(e^{-i\varphi_{(i)}} - e^{i\varphi_{(i-1)}})/[2e^{ik(i)l_{(i)}} \cos(\varphi_{(i)})],$$

$$t_{12} = e^{-ik(i-1)l_{(i)}}(e^{-i\varphi_{(i)}} + e^{-i\varphi_{(i-1)}})/[2e^{ik(i)l_{(i)}} \cos(\varphi_{(i)})],$$

$$t_{21} = e^{ik(i-1)l_{(i)}}(e^{i\varphi_{(i)}} + e^{i\varphi_{(i-1)}})/[2e^{-ik(i)l_{(i)}} \cos(\varphi_{(i)})],$$

$$t_{22} = e^{-ik(i-1)l_{(i)}}(e^{i\varphi_{(i)}} - e^{-i\varphi_{(i-1)}})/[2e^{-ik(i)l_{(i)}} \cos(\varphi_{(i)})],$$

$$l(i) = \text{INT}[i/2]D + \text{INT}[(i+1)/2]L,$$

$$k(i) = \begin{cases} k'_x, & \text{mod}(i, 2) = 0, \\ q_x, & \text{otherwise.} \end{cases}$$

$$\varphi_{(i)} = \begin{cases} \theta, & \text{mod}(i, 2) = 0, \\ \phi, & \text{otherwise.} \end{cases} \quad (7)$$

Where k'_x and q_x are the wave vector out and in the barrier along the x axis, the $\text{INT}[\]$ function returns the integer part

of a specified number. Then the angular dependence of transmission probability $T(\phi) = |a_{n+1}|^2$ for the system can be obtained. If we take $n=3$, it gives the same results to Ref. 13. For the double barrier case ($n=5$), it can be simplified as

$$T(\phi) = \frac{e^{-2ik'_x D - q(D+L)}(1 + e^{2i\theta})^2(1 + e^{2i\phi})^2}{A_1^2 + B_1^2}, \quad (8)$$

with

$$A_1 = e^{iq_x L} + e^{2i[\theta + q_x(D+L/2)]} + e^{2i[\phi + q_x(D+L/2)]} + 2e^{i[\theta + \phi + q_x(2D+L)]} + e^{2i(\theta + \phi + q_x L/2)} - 2e^{i(\theta + \phi + q_x L)} \quad (9)$$

and

$$B_1 = 4e^{i(\theta + \phi + k'_x L + q_x(D+L))}[\sin(\theta) + \sin(\phi)]\sin(q_x D). \quad (10)$$

Here L and D represent the width of the well and barrier, respectively.

B. Tunneling in bilayer graphene superlattice

For the bilayer graphene superlattice, the general solution to Eq. (3) can be expressed as

$$\varphi_1(x, y) = (a_i e^{ik_{ix}x} + b_i e^{-ik_{ix}x} + c_i e^{\kappa_{ix}x} + d_i e^{-\kappa_{ix}x}) e^{ik_y y},$$

$$\varphi_2(x, y) = s_i \left(a_i e^{ik_{ix}x + 2i\phi_i} + b_i e^{-ik_{ix}x - 2i\phi_i} - c_i h_i e^{\kappa_{ix}x} - \frac{d_i}{h_i} e^{-\kappa_{ix}x} \right) e^{ik_y y}, \quad (11)$$

where a_i , b_i , c_i , and d_i are the transmission amplitudes, and

$$s_i = \text{sgn}(V_i - E), \quad \hbar k_{ix} = \sqrt{2m|E - V_i|} \cos \phi_i,$$

$$\hbar k_{iy} = \sqrt{2m|E - V_i|} \sin \phi_i, \quad \kappa_{ix} = \sqrt{k_{ix}^2 + 2k_{iy}^2},$$

and

$$h_i = (\sqrt{1 + \sin^2 \phi_i} - \sin \phi_i)^2.$$

An important difference in the wave functions between the monolayer and the bilayer graphene is that in the latter case there are four possible solutions as shown in Eq. (11), two of which correspond to propagating waves and the other two to evanescent ones. Similar to the case of the monolayer graphene, utilizing continuity of the wave function at boundaries, the following transfer-matrix for the bilayer graphene structure is obtained:

$$\begin{pmatrix} 1 & b_1 & c_1 \\ -e^{2i\phi_1} & -b_1 e^{-2i\phi_1} & c_1 h_1 \\ ik_1 & -ik_1 b_1 & c_1 q_1 \\ -ik_1 e^{2i\phi_1} & ik_1 b_1 e^{-2i\phi_1} & c_1 q_1 h_1 \end{pmatrix} = \begin{pmatrix} 1 & 1 & 1 & 1 \\ e^{2i\phi_2} & e^{-2i\phi_2} & -h_2 & -1/h_2 \\ ik_2 & -ik_2 & q_2 & -q_2 \\ ik_2 e^{2i\phi_2} & -ik_2 e^{-2i\phi_2} & -q_2 h_2 & q_2/h_2 \end{pmatrix} S'_{(Z)} \times \begin{pmatrix} e^{ik_1 l(n)} & e^{-q_1 l(n)} \\ -e^{ik_1 l(n) + 2i\phi_1} & e^{-q_1 l(n)/h_1} \\ ik_1 e^{ik_1 l(n)} & -q_{(1)} e^{-q_1 l(n)} \\ -ik_1 e^{ik_1 l(n) + 2i\phi_1} & -q_1 e^{-q_1 l(n)/h_1} \end{pmatrix} \begin{pmatrix} a_{(n)} \\ d_{(n)} \end{pmatrix}, \quad (12)$$

where

$$S'_{(Z)} = S_{[Z=l(2)]}^{-1} S_{[Z=l(2)]}^* \cdots S_{[Z=l(i)]}^{-1} S_{[Z=l(i)]}^* \cdots S_{[Z=l(n-1)]}^{-1} S_{[Z=l(n-1)]}^*, \quad (13)$$

$$S_{[Z=l(i)]} = \begin{pmatrix} e^{ik_2 l(i)} & e^{-ik_2 l(i)} & e^{q_2 l(i)} & e^{-q_2 l(i)} \\ e^{ik_2 l(i) + 2i\phi_2} & e^{-ik_2 l(i) - 2i\phi_2} & -h_2 e^{q_2 l(i)} & e^{-q_2 l(i)/h_2} \\ ik_2 e^{ik_2 l(i)} & -ik_2 e^{-ik_2 l(i)} & q_2 e^{q_2 l(i)} & -q_2 e^{-q_2 l(i)} \\ ik_2 e^{ik_2 l(i) + 2i\phi_2} & -ik_2 e^{-ik_2 l(i) - 2i\phi_2} & -q_2 h_2 e^{q_2 l(i)} & q_2 e^{-q_2 l(i)/h_2} \end{pmatrix}, \quad (14)$$

$$S_{[Z=l(i)]}^* = \begin{pmatrix} e^{ik_1 l(i)} & e^{-ik_1 l(i)} & e^{q_1 l(i)} & e^{-q_1 l(i)} \\ e^{ik_1 l(i) + 2i\phi_1} & e^{-ik_1 l(i) - 2i\phi_1} & -h_1 e^{q_1 l(i)} & e^{-q_1 l(i)/h_1} \\ ik_1 e^{ik_1 l(i)} & -ik_1 e^{-ik_1 l(i)} & q_1 e^{q_1 l(i)} & -q_1 e^{-q_1 l(i)} \\ ik_1 e^{ik_1 l(i) + 2i\phi_1} & -ik_1 e^{-ik_1 l(i) - 2i\phi_1} & -q_1 h_1 e^{q_1 l(i)} & q_1 e^{-q_1 l(i)/h_1} \end{pmatrix}. \quad (15)$$

Then the angular dependence of a transmission probability for a bilayer graphene superlattice can be calculated as in the case of a monolayer graphene structure.

After transmission coefficients are obtained, the conductivity for the above systems can be calculated by means of the Buttiker formula,¹⁹

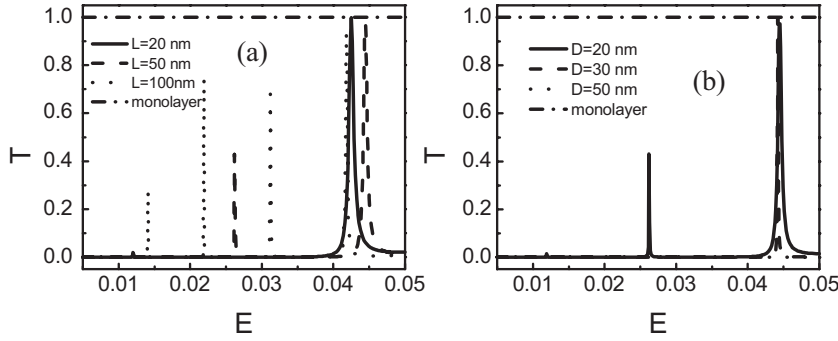


FIG. 2. Transmission probability T for normally incident electrons through double barriers and single well structure with monolayer and bilayer graphene as a function of Fermi energy E of the incident electrons. (a) For different well width L with the barrier heights $V_0=50$ meV and the barrier width $D=20$ nm and (b) for various barrier width D with $V_0=50$ meV and $L=50$ nm.

$$G = G_0 \int_{-\pi/2}^{\pi/2} T(E, \sqrt{2E} \sin \phi) \cos \phi d\phi, \quad (16)$$

where $G_0 = e^2 m v_F w / \hbar^2$. Combining Eqs. (16), (5), and (12), the various conductivities for two kinds of graphene superlattices can be obtained easily by the numerical calculations.

III. NUMERICAL RESULTS AND DISCUSSION

We first calculate the transmission probabilities of charge carriers through graphene structures with double barriers and a single well; the results are plotted in Figs. 2 and 3. Figure 2(a) presents the comparison of transmission probabilities of normally incident electrons between the monolayer and bilayer graphene structures as a function of the Fermi energy E of the incident electrons at various well widths. The solid line, dashed line, and dotted line correspond to the bilayer structure with $L=20$, 50, and 100 nm, respectively, and the dot-dashed line to the monolayer structure. It is seen from the figure that different features appear for two kinds of structures. For the monolayer graphene structure with the limit of high barriers $|V_0| \gg |E|$ under the condition of normal incidence ($\phi=0$), Eq. (4) can be simplified to $T=|t|^2$ with $t = e^{-2iD(k_x+q_x)}$. This means that the structure remains always perfectly transparent for normal incidence, which is independent on the well widths. The dot-dashed line in Fig. 2(a) exhibits the same feature. In fact, this transmission is not related to the thickness of barriers, either. Figure 2(b) displays the corresponding results at different barrier thicknesses with $L=50$ nm. The dot-dashed line represents the result of the monolayer graphene structure with various barrier thicknesses. Perfect transmission with $T=1$ is observed again. It is the feature unique to massless Dirac fermions and directly related to the Klein paradox.

However, the situation is completely different for the bilayer structure. With the change of the Fermi energy E of incident electrons, the resonant peaks appear (solid lines, dashed lines, and dotted lines in Fig. 2). The positions and numbers of resonant peaks change with the increase of well width. In contrast, they do not depend on thicknesses of the barriers because charge carriers in the bilayer graphene have a parabolic energy spectrum, which can be regarded as gapless semiconductors. In this case, scattering at the barrier is the same as for electrons described by the Schrödinger equation. It is well-known that the resonant tunneling can happen when electrons transport through the double-barrier structure of the semiconductor quantum well, where the resonant peaks are determined by quantum states in the well and independent of the barrier widths, so do present results for the bilayer graphene structure.

Although transmission probability for monolayer graphene at normal incidence is not related to the widths of the well and barrier, the angular dependence of transmission probability is. Figure 3 shows examples of such a transmission. Here, the concentrations of charge carriers are chosen as 0.5×10^{12} and $1 \times 10^{13} \text{ cm}^{-2}$ outside and inside the barrier, respectively, for all cases (such concentrations are most typical in experiments with graphene).¹³ This corresponds to the Fermi energy E of incident electrons approach 80 and 17 meV for the monolayer and the bilayer graphene, respectively, and wavelength $\lambda \approx 50$ nm. The band effective mass (m) for the corresponding bilayer graphene is taken as $0.035m_e$ and m_e is the bare electron mass. Figure 3(a) shows the angular dependence of transmission probability at different well widths for the monolayer graphene structure; (b) represents corresponding results for the bilayer graphene system. When well width is zero, the present structures degenerate into single barrier cases, in which the results [solid lines in Figs. 3(a) and 3(b)] are identical with those in Ref.

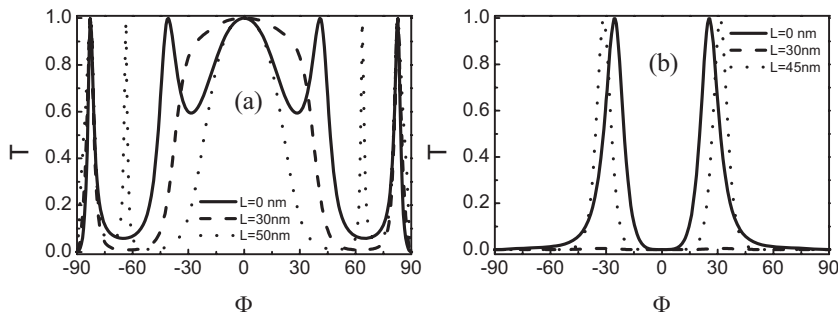


FIG. 3. Transmission probability T of electrons through double barriers and single well structures as a function of the incident angle for monolayer graphene with $V_0=200$ meV (a) and bilayer graphene with $V_0=50$ meV (b). Here $\lambda \approx 50$ nm for (a) and (b), and the potential widths D are taken as 50 nm (a) and 40 nm (b). The Fermi energy E of incident electrons is taken as 80 and 17 meV for (a) and (b), respectively.

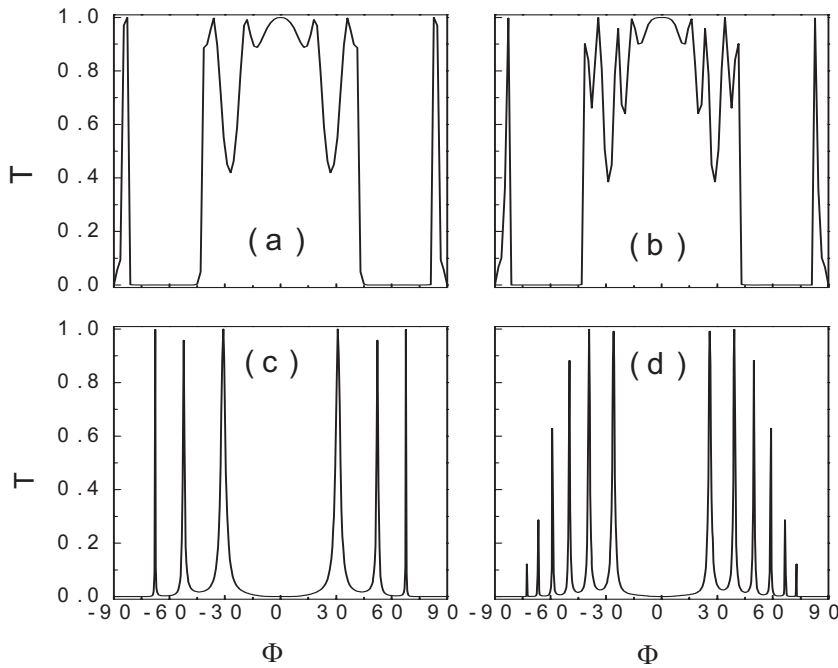


FIG. 4. Transmission probability T of electrons through five well structures [(a) and (c)] and ten well structures [(b) and (d)] as a function of the incident angle for monolayer graphene with $V_0=200$ meV [(a) and (b)] and bilayer graphene with $V_0=50$ meV [(c) and (d)]. $D=100$ nm and $L=30$ nm for the monolayer graphene structure; $D=10$ nm and $L=5$ nm for the bilayer graphene structure. The other parameters are taken the same as in Fig. 3.

13. With increasing L , the changes of angular dependence of transmission probability are very remarkable for two kinds of structure. This indicates that quantum tunneling in these materials becomes highly anisotropic due to the chiral nature of their quasiparticles, which is qualitatively different from the case of normal nonrelativistic electrons.

In contrast to the strictly normal incidence case ($\phi=0$), the angular dependence of transmission probability also depends on the number of wells. Figures 4(a) and 4(b) show such a transmission probability for the monolayer graphene superlattices with 5 and 10 wells, respectively. (c) and (d) represent the corresponding results for the bilayer graphene structure. Comparing them with the case of a single well (Fig. 3), we find that more peaks appear with the increase of well number. This indicates that the number of wells plays an important role in anisotropic transmission even for the monolayer graphene superlattice.

The property of the transmission probability directly leads to the fact that angularly averaged conductivities are related to the structure parameters of graphene systems. In Figs. 5(a) and 5(b), we plot the angularly averaged conductivities of graphene structures with double barriers and single well as a

function of well width for monolayer and bilayer graphene, respectively. Solid lines, dashed lines, and dotted lines correspond to the cases with various thicknesses of the barrier. We can clearly see that they all exhibit oscillatory behaviors with increased well width. It is interesting that the conductivities of the double-barrier structure in bilayer graphene can be driven to a very small value (near zero) by increasing well width. This can be understood from the angular dependence of transmission probability in Fig. 3(b). For example, the value of conductivity for a double-barrier structure of bilayer graphene at $L=30$ nm and $D=40$ nm [a point on the solid line in Fig. 5(b)] is a result of the integral for the dashed line in Fig. 3(b) through Eq. (16). Due to the change feature of the dashed line, the value of the integral for it is very small. In contrast, we can obtain a large value of integral for the dotted line in Fig. 3(b), which corresponds to the third peak of the dashed line in Fig. 5(b). This means that various angular dependences of transmission probability at different well widths are the origin of oscillatory conductivity with the change of well width.

At the same time, we find that the magnitude and period of oscillation also depend sensitively on thickness of barrier. With increase in barrier thickness, the oscillation becomes

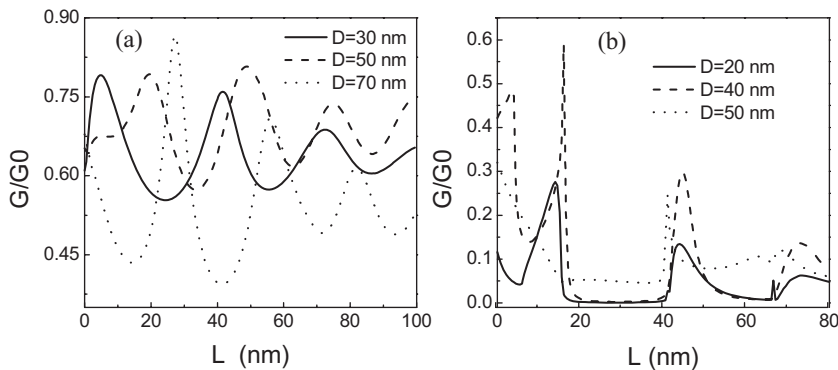


FIG. 5. Conductivity as a function of the well width L for double barriers and single well structures with different barrier widths at $V_0=220$ meV. (a) For monolayer and (b) for bilayer. The other parameters are taken the same as in Fig. 3.

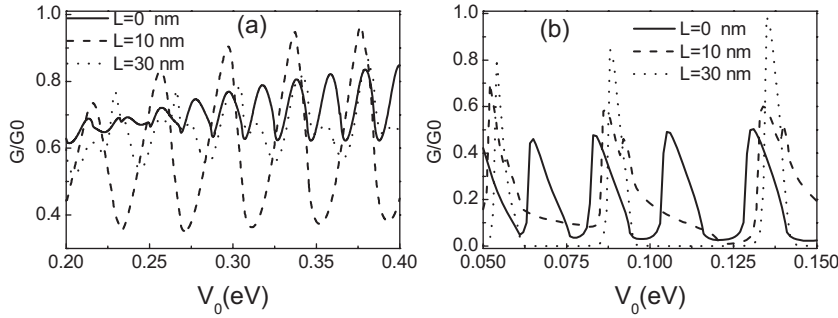


FIG. 6. Conductivity as a function of the barrier height V_0 for double barriers and single well structures with different well widths at $D=50$ nm for monolayer (a) and $D=40$ nm for bilayer (b). The other parameters are taken the same as in Fig. 3.

stronger for the monolayer graphene structure. For the bilayer graphene structure, the change is much more complex. At the thin barrier, the oscillation becomes stronger with increasing D . However, it decreases at the thick barrier, which exhibits the same features as in the resonant tunneling structure of the semiconductor with double barriers again. Furthermore, the feature of oscillation is also related to the height of barrier. This can be seen clearly from Fig. 6.

Figures 6(a) and 6(b) show the conductivities as a function of barrier height V_0 with different well widths at $D=50$ nm for the monolayer and bilayer graphene structures, respectively. The conductivities are also an oscillating function of V_0 , although the transmission probability of normally incident electrons is always 1 for monolayer graphene. This is because the angular dependences of transmission probabilities for the above systems are related to the wave vector q_x . For example, in the limit of high barriers $|V_0| \gg |E|$, $T(\phi) = \cos^2 \phi / [1 - \cos^2(q_x D) \sin^2 \phi]$ for the monolayer junction with a single barrier.¹³ This relation yields resonance conditions $q_x D = n\pi$. That is to say, $T(\phi)$ is an oscillating function of q_x and q_x is determined by V_0 . This leads to that $T(\phi)$ and conductivities are also the oscillating function of V_0 . Their periodicities of oscillation are determined by resonance conditions. From Fig. 6(a), we can also find that the oscillation magnitudes of conductivities are sensitive to the modulation of well width for the monolayer graphene structure even to the existence of the Klein tunneling. For example, the ratio of maximum to minimum of magnitude is 2.6:1 for such a structure at $V_0=0.35$ eV and $L=30$ nm. In

contrast, for the bilayer graphene structure, the resonant tunneling feature is found again with the modulation of well width, which is similar to the semiconductor structure with double barriers. This means that we can modulate conductivities by changing the structure parameters for two kinds of graphene systems.

The above results of the conductivities are only applicable to a structure with double barriers and a single well. If the number of wells is increased, the results will become more interesting. Figure 7 shows conductivity as a function of the Fermi energy E of incident electrons for the monolayer graphene superlattice with various numbers of wells. The solid line, dashed line, dotted line, and dot-dashed line correspond to the cases with 1, 2, 5, and 10 wells, respectively. Although the oscillation period does not change, the magnitudes of oscillation are tuned largely with the increase of well number. For example, the ratio of maximum to minimum of magnitude can reach 12:1 at the present structure with 10 wells. As for the bilayer graphene structure, the magnitude and period all can be changed largely with the increase of well number. The corresponding results are plotted in Fig. 8. It exhibits similar features to those in the semiconductor superlattice with multiple quantum wells.

IV. SUMMARY

Based on the transfer-matrix method, we have investigated the transport properties of charge carriers through graphene superlattices consisting of monolayer and bilayer

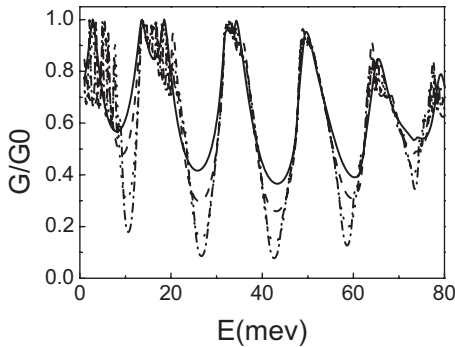


FIG. 7. Conductivity as a function of the Fermi energy E of incident electrons for the monolayer graphene superlattice with different numbers of wells. Solid line, dashed line, dotted line, and dot-dashed line correspond to 1, 2, 5, and 10 well structures, respectively. The other parameters are taken the same as in Fig. 4.

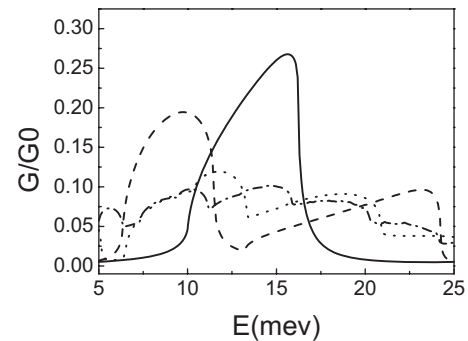


FIG. 8. Conductivity as a function of the Fermi energy E of incident electrons for the bilayer graphene superlattice with different numbers of wells. Solid line, dashed line, dotted line, and dot-dashed line correspond to 1, 2, 5, and 10 well structures, respectively. The other parameters are taken the same as in Fig. 4.

graphene. The normal incidence and angularly dependent transmission probabilities for two kinds of graphene structure have been calculated. It is shown that the angular dependence of the transmission probability is directly related to structure parameters, even if the Klein tunneling exists in the monolayer graphene structure. In contrast to the monolayer graphene structure, the transmission of the bilayer graphene system exhibits similar properties to those in the semiconductor superlattice. Various angular dependences of transmission probability have angularly averaged conductivities that depend sensitively on the thickness and height of the barrier as well as the width and number of wells. This means that the angularly averaged conductivities in monolayer and

bilayer graphene superlattices can be controlled by changing the structure parameters though the Klein tunneling exists. We hope that our theoretical results can provide an important reference to the design of electron devices based on graphene materials.

ACKNOWLEDGMENTS

This work was supported by the National Natural Science Foundation of China (Grant No. 10674017) and the National Key Basic Research Special Foundation of China under Grant 2007CB613205. The project was also sponsored by NCET and RFDP.

*Corresponding author; zhangxd@bnu.edu.cn

¹K. S. Novoselov, A. K. Geim, S. V. Morozov, D. Jiang, Y. Zhang, S. V. Dubonos, I. V. Grigorieva, and A. A. Firsov, *Science* **306**, 666 (2004).

²P. R. Wallace, *Phys. Rev.* **71**, 622 (1947).

³For a review, see T. Ando, *J. Phys. Soc. Jpn.* **74**, 777 (2005).

⁴K. S. Novoselov, A. K. Geim, S. V. Morozov, D. Jiang, M. I. Katsnelson, I. V. Grigorieva, S. V. Dubonos, and A. A. Firsov, *Nature (London)* **438**, 197 (2005); *Nat. Phys.* **2**, 177 (2006).

⁵Y. Zhang, Y. W. Tan, H. L. Stormer, and P. Kim, *Nature (London)* **438**, 201 (2005).

⁶V. P. Gusynin and S. G. Sharapov, *Phys. Rev. Lett.* **95**, 146801 (2005).

⁷E. McCann and V. I. Falko, *Phys. Rev. Lett.* **96**, 086805 (2006).

⁸Y. Zheng and T. Ando, *Phys. Rev. B* **65**, 245420 (2002).

⁹Y. Zhang, J. P. Small, M. E. S. Amori, and P. Kim, *Phys. Rev. Lett.* **94**, 176803 (2005).

¹⁰K. S. Novoselov, E. McCann, S. V. Morozov, V. I. Falko, M. I. Katsnelson, U. Zeitler, D. Jiang, F. Schedin, and A. K. Geim, *Nat. Phys.* **2**, 177 (2006).

¹¹C. W. J. Beenakker, *Phys. Rev. Lett.* **97**, 067007 (2006).

¹²S. Bhattacharjee and K. Sengupta, *Phys. Rev. Lett.* **97**, 217001 (2006).

¹³M. I. Katsnelson, K. S. Novoselov, and A. K. Geim, *Nat. Phys.* **2**, 620 (2006).

¹⁴O. Klein, *Z. Phys.* **53**, 157 (1929).

¹⁵W. Greiner, B. Mueller, and J. Rafelski, *Quantum Electrodynamics of Strong Fields* (Springer, Berlin, 1985).

¹⁶R. K. Su, G. C. Siu, and X. Chou, *J. Phys. A* **26**, 1001 (1993).

¹⁷N. Dombey and A. Calogeracos, *Phys. Rep.* **315**, 41 (1999).

¹⁸P. Krekora, Q. Su, and R. Grobe, *Phys. Rev. Lett.* **92**, 040406 (2004).

¹⁹M. Buttiker, *Phys. Rev. Lett.* **57**, 1761 (1986).